ДГКС ASES | E-37
Kongres 2026
Congress 2026

doi: 10.67563/ASESCONF2026055S

Dženisa Šaini[1], Ricardo Branco[2], David Andrade[1,3], Mariela Mendez-Morales[1], João Pedro Martins[1], Luís Simões da Silva[1]

ON DED-ARC HYBRID TRANSITIONAL JOINTS IN STRUCTURAL APPLICATIONS

Summary: This paper investigates the fatigue performance of a hybrid transitional joint in an I-girder stiffener using DED-Arc AM46 steel from a material and detail perspective. High-cycle fatigue (HCF) tests were performed on machined/polished specimens extracted in horizontal and vertical directions relative to the welding beads. The obtained results were used to define the material S-N curve, showing behavior comparable to conventional S355 steel and a fatigue limit of 371 MPa at 2×10^6 cycles. The hybrid joint was evaluated using linear static finite element analysis and the Theory of Critical Distances. For all analyzed geometries and service load levels, the effective stresses remained below the fatigue limit, indicating infinite life under the considered loading. Experimental validation is required to confirm this behavior under realistic manufacturing conditions.

Keywords: directed energy deposition-arc, AM46 steel, high-cycle fatigue, S-N curve, hybrid transitional joint, fatigue life

O DED-ARC HIBRIDNIM SPOJEVIMA U KONSTRUKTIVNOJ PRIMENI

Rezime: Ovaj rad istražuje otpornost na zamor hibridnog spoja integrisanog u poprečno ukrućenje I-nosača kroz primenu DED-Arc AM46 čelika, analiza se sprovodi na nivou materijala i konstruktivnog detalja. Visokociklična ispitivanja su sprovedena na mašinski obrađenim i poliranim uzorcima orijentisanim horizontalno i vertikalno u odnosu na pravac nanošenja materijala. Na osnovu rezultata definisana je S-N kriva materijala. Rezultati pokazuju ponašanje uporedivo sa konvencionalnim S355 čelikom, uz trajnu dinamičku čvrstoću od 371 MPa pri 2×10^6 ciklusa. Hibridni spoj je analiziran primenom linearne statičke metode konačnih elemenata i teorije kritičnih rastojanja. Za razmatrane geometrije i nivoe eksploatacionog opterećenja, efektivni naponi su ispod trajne dinamičke čvrstoće, što ukazuje na beskonačan zamorni vek pri razmatranom opterećenju. Eksperimentalna ispitivanja su potrebna u daljem radu kako bi se procenio uticaj procesa izrade na otpornost na zamor.

Ključne reči: directed energy deposition-arc, AM46 čelik, visokociklični zamor, S-N kriva, hibridan spoj, zamorni vek

---

[1] University of Coimbra, ISISE, ARISE, Department of Civil Engineering, Coimbra, Portugal, dzenisa.saini@student.uc.pt
[2] University of Coimbra, CEMMPRE, ARISE, Department of Mechanical Engineering, Portugal
[3] TEMA - Centre for Mechanical Technology and Automation, Department of Mechanical Engineering, University of Aveiro, Campus Universitário de Santiago, Aveiro, Portugal

1. INTRODUCTION

Steel structures rely extensively on welded joints and connections, which often introduces geometric discontinuities, residual stresses and fabrication imperfections that result in stress concentrations, leading to reduced fatigue life [1]. In steel bridges, fatigue damage is mainly caused by cyclic traffic-induced stress histories [2], with welded details such as transverse stiffener-to- I-girder connections, often identified as fatigue-critical regions [2-4]. Simultaneously, additive manufacturing is increasingly being explored as an alternative fabrication approach for producing optimized structural details with reduced stress concentrations, improved geometric efficiency, fatigue performance and long-term durability [3].

Directed Energy Deposition-Arc (DED-Arc) is a promising fabrication technology for large-scale steel applications, offering high deposition rates, material efficiency and reduced production lead time [5]. Carbon steel feedstocks, such as AM46 steel, further support its structural and economic viability. While DED-Arc enables complex and customized geometries, process-induced features such as surface irregularities, porosity, residual stresses, material anisotropy, and microstructural heterogeneity may affect its fatigue behavior [5-7].

Several studies have investigated the high-cycle fatigue (HCF) behavior of DED-Arc steels, mainly ER70S-6 low carbon steel and stainless steels. Despite Ermakova et al. [7] reporting orientation-dependent behavior under uniaxial, torsional and multiaxial loading, recent research has shown that build orientation has limited influence on fatigue performance [8-10]. On the contrary, surface condition was identified as the dominant factor affecting fatigue behavior, with as-built irregularities leading to earlier crack initiation and reducing fatigue life compared to machined specimens [6,11]. Post-processing techniques, such as machining and rolling, improve fatigue performance by reducing surface waviness and stress concentrations. Furthermore, rolling additionally introduces beneficial compressive residual stresses [12,13]. Porosity reduces fatigue strength by acting as a crack initiation site, particularly in corrosive environments [14].

Existing studies on low carbon AM46 steel are rare in the literature and have mainly addressed the influence of fabrication parameters on microstructure and monotonic mechanical properties [15], while its cyclic behavior remains insufficiently understood, particularly at the component level. This paper assesses the feasibility of advancing the design and fabrication of a hybrid transitional joint integrated into an I-girder transverse stiffener, representative of a small-scale bridge girder detail, through the adoption of emerging manufacturing technologies and materials. The study is based on the detailed characterization of the HCF behavior of DED-Arc AM46 carbon steel and uses these findings to quantify the fatigue performance of the proposed transitional joint detail.

2. METHODOLOGY

2.1. EXPERIMENTAL PROCEDURE

AM46 steel wire supplied by Böhler Voestalpine, and having a diameter of 1.2 mm, was used as the feedstock material. The material was manufactured using an ABB IRB 4600 robot integrated with a Fronius TPS 400i welding machine and equipped with Cold Metal Transfer (CMT) technology. The nominal chemical composition and mechanical properties provided in the supplier’s data sheet are summarized in Table 1 and Table 2, respectively.

Table 1: Nominal chemical composition [wt.%] of AM46 steel wire [16]

C	Mn	Si
0.1	1.7	1.0

Table 2: Mechanical properties of AM46 steel wire [16]

Yield strength f_y [MPa]	Tensile strength f_u [MPa]	Failure strain ε_u [%]
480	580	24

Using the process parameters summarized in Table 3, 390 × 200 × 8.1 mm walls were fabricated using a single-bead deposition strategy, as illustrated in Figure 1(a), where each layer consisted of one continuous welding pass along the wall length. To achieve a more uniform heat distribution, the deposition direction was alternated between successive layers i.e., the first layer was deposited from right to left and the following from left to right.

An M21 shielding gas mixture consisting of 82% Ar and 18% CO_2 was applied throughout the deposition process at a constant flow rate of 20 L/min. Thermal history was characterized through the $\Delta t_{8/5}$ cooling time, corresponding to the cooling interval between 800 °C and 500 °C obtained from the recorded temperature profiles. The interpass temperature was maintained below 250 °C during deposition.

Table 3: Deposition parameters used in the fabrication of wall plates

Wire diameter [mm]	Current [A]	Voltage [V]	Welding speed [mm/s]	Wire feed speed [m/min]	Heat input [kJ/mm]
1.2	150	21.3	6.0	4.7	0.5

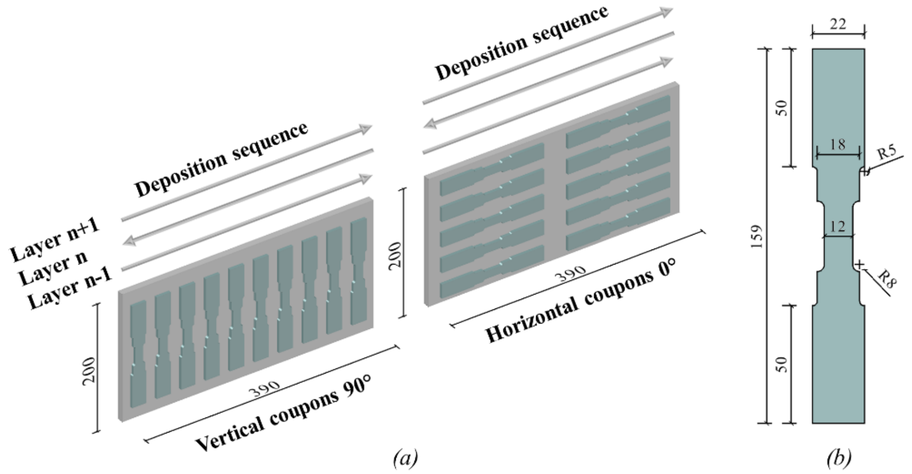

Figure 1: (a) Geometry and deposition strategy of the DED-Arc walls and schematic layout used for specimen extraction; (b) geometry of HCF specimens (units: millimeters)

The HCF specimens, with the geometry shown in Figure 1(b), were extracted from DED-Arc wall plates in two orientations relative to the welding beads, with nominal thickness of 5 mm: horizontal (0°) and vertical (90°). Fatigue tests were performed under force-controlled loading at a stress ratio R = 0, with stress levels ranging between 70% and 90% of the tensile strength. Four stress ranges were considered, with three repetitions conducted at each stress level. In total, 18 specimens were tested, 9 specimens per orientation.

2.2. HYBRID TRANSITIONAL JOINT

A linear static finite element analysis was conducted in Abaqus to investigate a hybrid transitional joint incorporated within a central transverse stiffener of a 6 m long S355 steel I-girder, as shown in Figure 2. The girder was designed in accordance with EN 1993-1-1, EN 1993-1-8 and EN 1993-1-9 [17-19] for a stress range of $\Delta\sigma$ = 250 MPa (R = 0). The hybrid joint was formed by replacing the lower portion of the stiffener with a DED-Arc-fabricated component, while the remaining stiffeners were conventionally welded. Two DED-Arc component geometries were investigated, with bottom widths of 40 mm and 150 mm, respectively. Both components had a height of 40 mm and a length of 130 mm. The numerical models were based on idealized geometries, and did not account for surface irregularities, porosity, residual stresses, material anisotropy, and microstructural heterogeneity typically associated with the DED-Arc manufacturing process.

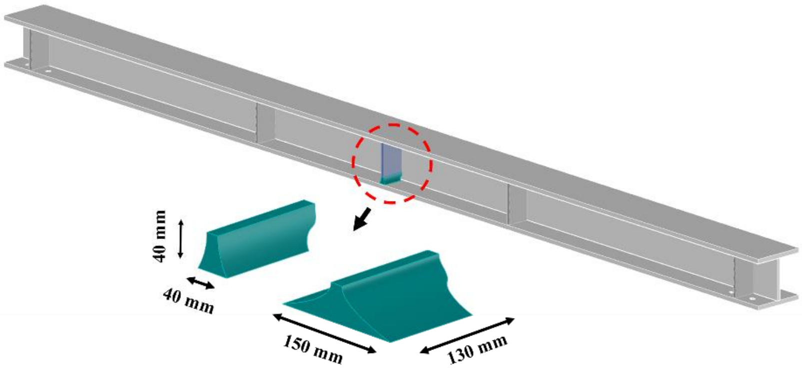

Figure 2: Hybrid transitional joint and corresponding DED-Arc component geometries

The finite element model included two materials. DED-Arc AM46 carbon steel was used for the additively manufactured component, with material properties taken from the previous mechanical characterization. To obtain a more conservative numerical model, the properties of the horizontal specimens were adopted. S355 steel was used for the remaining girder components, with material properties defined according to EN 10025-3 [20]. Both materials were modeled as linear elastic, defined by the Young's modulus and Poisson's ratio, the latter taken as 0.3 for each. The corresponding material properties are summarized in Table 4.

Table 4: Mechanical properties of DED-Arc AM46 and S355 steel

Material		Young's modulus E [GPa]	Yield strength f_y [MPa]	Tensile strength f_u [MPa]	Failure strain ε_u [%]
S355		210	345	470	22
DED-Arc	Vertical	183	407	505	16
	Horizontal	180	407	517	17

The I-girder was modeled as a simply supported beam subjected to four-point bending, with load application points located at 1 m from midspan, see Figure 3(a). The displacement-controlled analysis was performed for two service load levels, corresponding to 60% and 80% of the beam resistance [21, 22]. The force level associated with each load level was determined, and the corresponding vertical displacement was then applied in the finite element model. These applied vertical displacements were 14.04 mm and 18.86 mm for the 60% and 80% service load levels, respectively. The left support was defined as pinned, while the right support was defined as a roller, allowing longitudinal movement and preventing restraint-induced tensile stresses in the girder flange.

The finite element mesh primarily consisted of hexahedral elements (C3D8R), while tetrahedral elements (C3D10) were used in geometrically complex regions where a structured mesh could not be generated, see Figure 3(b). Local mesh refinement was applied in the critical stress region of the bottom flange and DED-Arc component. A mesh sensitivity study was performed through progressive refinement, with the final mesh defined by an element size of 4 mm in the bottom flange and in the longitudinal direction of the DED-Arc component, and 1.5 mm in the transverse direction of the DED-Arc component.

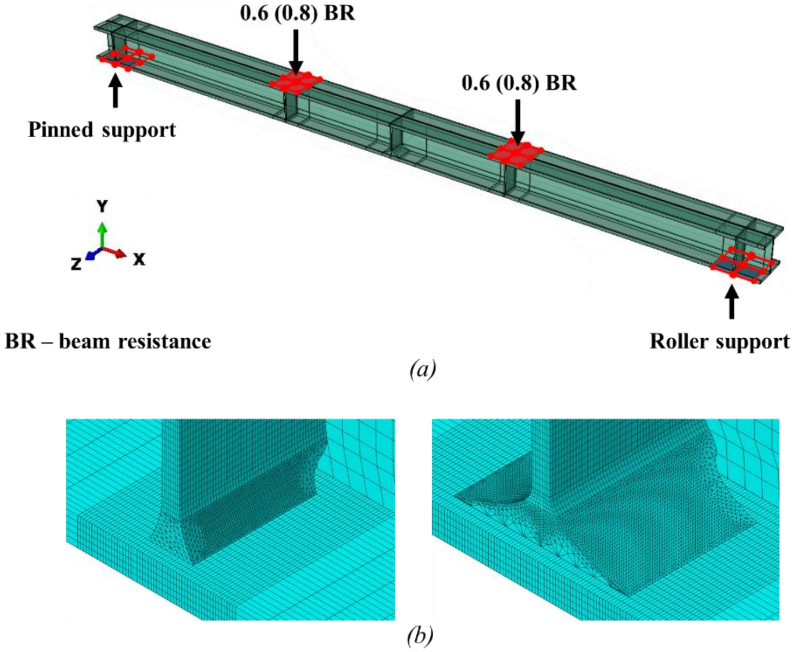

Figure 3: Finite element model: (a) support and load application points; (b) finite element mesh

2.3. ANALYSIS PROCEDURE

The fatigue analysis combines the experimentally derived S-N curve of the DED-Arc material with the linear-elastic stress field obtained from the I-girder finite element model. The critical stress concentrator in the hybrid joint is identified based on the maximum principal stress, and the local stress profile is extracted along a path perpendicular to the toe line at that location.

To account for the mesh-induced stress singularities affecting the extracted stress profile, the Theory of Critical Distances (TCD) is applied to determine representative effective stresses using the Point Method (PM) and Line Method (LM) [23]. Both methods are formulated based on the elastic stress field near the critical location. The el Haddad parameter a_0 [24], representing the material characteristic length, is determined using Eq. (1) and then used to obtain the critical distances D for the two methods according to Eq. (2) and Eq. (3). In the Point Method, effective stress is obtained from the extracted stress profile as the stress value located at the critical distance D_{PM} from the maximum-stress location. In the Line Method, effective stress is determined from the same stress profile by integrating stress distribution over the critical distance D_{LM} and normalizing it by D_{LM}.

The effective stress ranges obtained from the PM and LM are used as input to the experimentally derived S-N curve of the DED-Arc material to determine the fatigue life of each geometric configuration. This enables the fatigue performance of the hybrid transitional joint to be estimated and compared across the investigated configurations.

$$a_0 = \frac{1}{\pi}\left(\frac{\Delta K_{th}}{\Delta \sigma_0}\right) \tag{1}$$

where:
π is the mathematical constant,
ΔK_{th} is the stress intensity factor range at the threshold,
$\Delta\sigma_0$ is the fatigue strength of the unnotched part.

$$D_{PM} = \frac{a_o}{2} \tag{2}$$

$$D_{LM} = 2a_0 \tag{3}$$

Note that, the stress intensity factor range at the threshold, ΔK_{th}, is not a single material constant, as it depends on factors such as stress ratio, microstructure, mean stress, temperature, and environmental conditions.

3. RESULTS & DISCUSSION

3.1. HIGH-CYCLE FATIGUE BEHAVIOR

The applied stress amplitudes were defined based on the tensile strengths of the horizontal and vertical specimens, which were 517 MPa and 505 MPa, respectively, as shown in Table 4. Specimens that reached an infinite life defined at $N_f \geq 2 \times 10^6$ were retested at a higher stress amplitude. The stress amplitude-number of cycles to failure relationship is presented in Figure 4, along with literature data for S355 structural steel [25]. The figure also includes the fitted experimental S-N curve corresponding to a 50% survival probability, shown as a solid black line, and the 2.5% and 97.5% survival bounds, shown as dashed red lines and obtained by shifting the 50% survival curve by two standard deviations while keeping the same slope. The fatigue limit, defined at 2×10^6cycles on the 50% fitted curve, corresponds to a stress amplitude of 185 MPa, or equivalently a stress range of 371 MPa. The experimental results show good agreement with the fatigue behavior reported for S355 structural steel [25], and although some scatter is observed in both orientations, the horizontal and vertical specimens exhibit similar fatigue behavior overall.

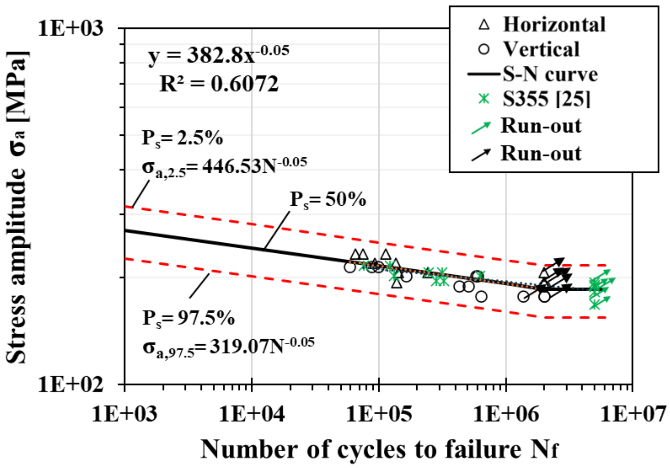

Figure 4: HCF experimental results with fitted S-N curve and 2.5% and 97.5% survival probability bounds

3.2. STRESS ANALYSIS

The maximum principal stresses in the DED-Arc component, as per the finite element analysis, were identified in the vicinity of the end of the transition zone, as illustrated in Figure 5(a), corresponding to the critical weld toe region. From this location, a stress evaluation path was defined perpendicular to the toe line and extending away from the DED-Arc component. Figure 5(b) illustrates the extracted stress profiles for the two DED-Arc component geometries under investigation, corresponding to widths of 40 mm and 150 mm. The labels 0.6BR and 0.8BR refer to the applied service load levels, corresponding to 60% and 80% of the beam resistance, respectively.

The critical distances required for the TCD analysis were calculated according to Eqs. (1)-(3), using $\Delta K_{th} = 16.12\ \text{MPa}\sqrt{\text{m}}$, obtained from the crack growth results reported by Mendez-Morales et al. [26] for WAAM carbon steel and a stress ratio of R = 0.05. The extracted stress profiles were then analyzed using TCD to determine effective stresses, as illustrated in Figure 5(c), with the corresponding values summarized in Table 5.

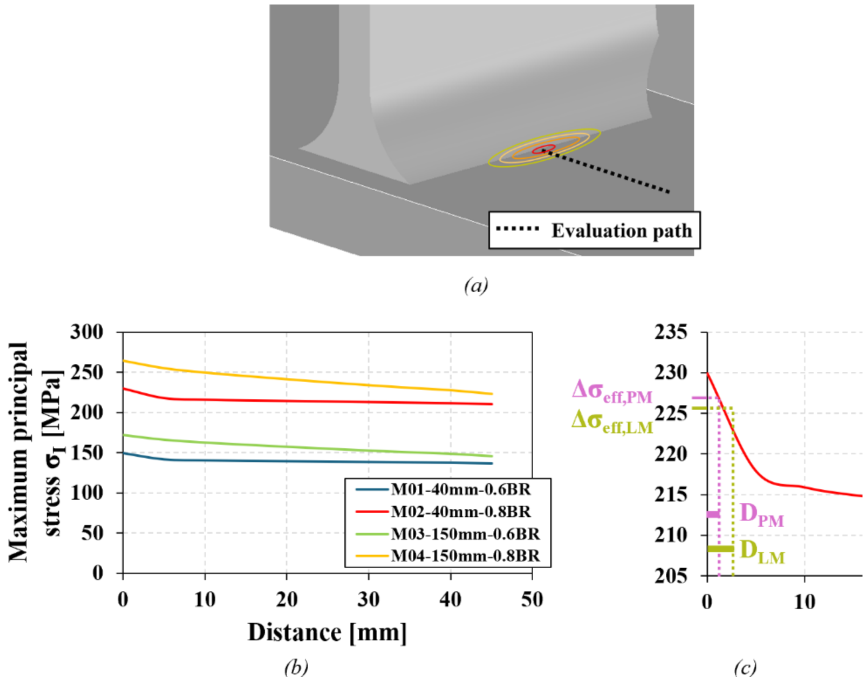

Figure 5: (a) location of the maximum principal stresses and evaluation path; (b) extracted FE stress profiles; (c) TCD-based effective stress evaluation using PM and LM

Table 5: TCD effective stresses for the DED-Arc components

	60% Beam Resistance		80% Beam Resistance	
	40 mm	150 mm	40 mm	150 mm
$\Delta\sigma_{eff,PM}$ [MPa]	149.3	229.2	172.0	264.3
$\Delta\sigma_{eff,LM}$ [MPa]	148.9	228.6	171.7	263.8

The TCD effective stress ranges were compared with the fatigue limit defined at 2×10^6 cycles obtained from the 97.5% fitted S-N curve, which represents the design curve corresponding to a 2.5% probability of failure. This fatigue limit corresponds to stress ranges of 309 MPa. Since effective stress ranges obtained for investigated configurations remain below this fatigue limit, configurations are considered to operate below the endurance limit. Accordingly, infinite life is assumed for the applied service load levels.

It should be noted that this study represents a preliminary fatigue assessment based on constant-amplitude loading, with stress ranges derived from a linear static finite element model. Further work will consider variable-amplitude cyclic loading and realistic manufacturing conditions.

4. CONCLUSIONS

This paper investigated the fatigue performance of a hybrid transitional joint incorporated within an I-girder stiffener, supported by high-cycle fatigue characterization of DED-Arc AM46 steel. High-cycle fatigue tests were conducted on machined/polished extracted in vertical and horizontal orientations. The tests were performed under force-controlled loading at a stress ratio of R = 0, with stress levels ranging from 70% to 90% of the tensile strength.

The hybrid transitional joint was numerically analyzed within a 6 m long S355 steel I-girder. The joint was incorporated within the central transverse stiffener by replacing its lower portion with a DED-Arc-fabricated component, while the remaining stiffeners were conventionally welded. Two DED-Arc component geometries were analyzed, corresponding to widths of 40 mm and 150 mm. The numerical model was subjected to displacement-controlled four-point bending at two service load levels, representing 60% and 80% of the beam resistance.

Based on the results obtained in this study, the following conclusions can be drawn:

- The tested material showed good agreement with literature data for conventional S355 steel, indicating comparable fatigue performance for the analyzed DED-Arc material. The fatigue limit, defined at 2×10^6cycles on the fitted S-N curve corresponding to a 50% survival probability, is a stress range of 371 MPa.
- The finite element analysis identified the end of the transition zone at the flange as the critical region of the hybrid transitional joint. Following the TCD-based evaluation, the effective stresses obtained for both DED-Arc geometries and service load levels were below the material fatigue limit. Accordingly, the investigated configurations remain below the endurance limit, indicating infinite life under the considered service loading. This conclusion applies to the idealized numerical geometry used in the finite element model.

Surface irregularities, porosity, residual stresses, material anisotropy or microstructural heterogeneity associated with the DED-Arc process were not included in the analysis. These manufacturing-induced features may accelerate fatigue crack initiation and reduce fatigue performance compared with the idealized model. Therefore, although the numerical results indicate promising behavior of the analyzed hybrid transitional joint, experimental testing of fabricated specimens is required to confirm its fatigue performance under realistic manufacturing and loading conditions.

ACKNOWLEDGMENTS

This work was funded by the Research Fund for Coal and Steel under grant agreement 101112614 — IAMFat. This work was also supported by FCT / MCTES through national funds (PIDDAC) under the R&D Unit Institute for Sustainability and Innovation in Structural Engineering (ISISE), under reference UID/04029/Institute for Sustainability and Innovation in Structural Engineering (ISISE), CEMMPRE under the project UIDB/00285/2020, TEMA under the project UID 00481/2025, and under the Associate Laboratory Advanced Production and Intelligent Systems ARISE under reference LA/P/0112/2020.

REFERENCES

[1] Haghani, R., Al-Emrani, M., & Heshmati, M. (2012). Fatigue-Prone Details in Steel Bridges. *Buildings*, *2*(4), 456–476. https://doi.org/10.3390/buildings2040456

[2] Fricke, W. (2015). Recent developments and future challenges in fatigue strength assessment of welded joints. *Proceedings of the Institution of Mechanical Engineers, Part C: Journal of Mechanical Engineering Science*, *229*(7), 1224–1239. https://doi.org/10.1177/0954406214550015

[3] Skoglund, O., & Leander, J. (2022). A numerical evaluation of new structural details for an improved fatigue strength of steel bridges. *International Journal of Fatigue*, *160*, 106866. https://doi.org/10.1016/j.ijfatigue.2022.106866

[4] Wang, C., Wang, Y., Duan, L., & de Corte, W. (2022). Distortion-induced fatigue behavior of vertical stiffener web gaps in steel girder bridges. *Thin-Walled Structures*, *180*, 109892. https://doi.org/10.1016/j.tws.2022.109892

[5] Evans, S. I., Wang, J., Qin, J., He, Y., Shepherd, P., & Ding, J. (2022). A review of WAAM for steel construction – Manufacturing, material and geometric properties, design, and future directions. *Structures*, *44*, 1506–1522. https://doi.org/10.1016/j.istruc.2022.08.084

[6] Huang, C., Li, L., Pichler, N., Ghafoori, E., Susmel, L., & Gardner, L. (2023). Fatigue testing and analysis of steel plates manufactured by wire-arc directed energy deposition. *Additive Manufacturing*, *73*, 103696. https://doi.org/10.1016/j.addma.2023.103696

[7] Ermakova, A., Razavi, N., Berto, F., & Mehmanparast, A. (2023). Uniaxial and multiaxial fatigue behaviour of wire arc additively manufactured ER70S-6 low carbon steel components. *International Journal of Fatigue*, *166*, 107283. https://doi.org/10.1016/j.ijfatigue.2022.107283

[8] Wächter, M., Leicher, M., Hupka, M., Leistner, C., Masendorf, L., Treutler, K., Kamper, S., Esderts, A., Wesling, V., & Hartmann, S. (2020). Monotonic and Fatigue Properties of Steel Material Manufactured by Wire Arc Additive Manufacturing. *Applied Sciences*, *10*(15), 5238. https://doi.org/10.3390/app10155238

[9] Duraisamy, R., Kumar, S. M., Kannan, A. R., Shanmugam, N. S., & Sankaranarayanasamy, K. (2021). Fatigue Behavior of Austenitic Stainless Steel 347 Fabricated via Wire Arc Additive Manufacturing. *Journal of Materials Engineering and Performance*, *30*(9), 6844–6850. https://doi.org/10.1007/s11665-021-06033-3

[10] Ayan, Y., & Kahraman, N. (2022). Bending fatigue properties of structural steel fabricated through wire arc additive manufacturing (WAAM). *Engineering Science and Technology, an International Journal*, *35*, 101247. https://doi.org/10.1016/j.jestch.2022.101247

[11] Bartsch, H., Kühne, R., Citarelli, S., Schaffrath, S., & Feldmann, M. (2021). Fatigue analysis of wire arc additive manufactured (3D printed) components with unmilled surface. *Structures*, *31*, 576–589. https://doi.org/10.1016/j.istruc.2021.01.068

[12] Dirisu, P., Supriyo, G., Martina, F., Xu, X., & Williams, S. (2020). Wire plus arc additive manufactured functional steel surfaces enhanced by rolling. *International Journal of Fatigue*, *130*, 105237. https://doi.org/10.1016/j.ijfatigue.2019.105237

[13] Ghafoori, E., Dahaghin, H., Diao, C., Pichler, N., Li, L., Mohri, M., Ding, J., Ganguly, S., & Williams, S. (2023). Fatigue strengthening of damaged steel members using wire arc additive manufacturing. *Engineering Structures*, *284*, 115911. https://doi.org/10.1016/j.engstruct.2023.115911

[14] Ron, T., Levy, G. K., Dolev, O., Leon, A., Shirizly, A., & Aghion, E. (2020). The Effect of Microstructural Imperfections on Corrosion Fatigue of Additively Manufactured ER70S-6 Alloy Produced by Wire Arc Deposition. *Metals*, *10*(1), 98. https://doi.org/10.3390/met10010098

[15] Tankova, T., Zhu, C., el Bamby, H., Monteiro, K., Sabari, S., da Silva, L. S., & Andrade, D. G. (2026). Influence of metal transfer modes and process conditions on WAAM-fabricated AM46 carbon steel walls. *Structures*, *84*, 110936. https://doi.org/10.1016/j.istruc.2025.110936

[16] Voestalpine Böhler Welding. 3Dprint AM 46: S460 - 8MnSi7 - 1.5113 2019.

[17] EN 1993-1-1, Eurocode 3: Design of Steel Structures - Part 1-1: General Rules and Rules for Buildings, CEN, Brussels, 2005.

[18] EN 1993.1.8 - Design of steel structures - Part 1-8: Design of joints, European Committee for Standardization, 2005.

[19] EN 1993.1.9 - Design of steel structures - Part 1-9: Fatigue, European Committee for Standardization, 2005.

[20] EN 10025-3 - Hot rolled products of structural steels - Part 3: Technical delivery conditions for normalized/normalized rolled weldable fine grain structural steels, European Committee for Standardization, 2019.

[21] Caner, A., & Zia, P. (1998). Behavior and Design of Link Slabs for Jointless Bridge Decks. *PCI Journal*, *43*(3), 68–80. https://doi.org/10.15554/pcij.05011998.68.80

[22] Bouassida Y, Bouchon E, Crespo P, Croce P, Davaine L, Denton S, Feldmann M, Frank R, Hanswille G, Hensen W, Kolias B, Malakatas N, Mancini G, Ortega Cornejo M, Sedlacek G, Tsionis G, authors Athanasopoulou A, Poljansek M, Pinto Vieira A, editors. Bridge Design to Eurocodes – Worked examples. EUR 25193 EN. Luxembourg (Luxembourg): Publications Office of the European Union; 2012. JRC68415

[23] Taylor, D. (1999). Geometrical effects in fatigue: a unifying theoretical model. *International Journal of Fatigue*, *21*(5), 413–420. https://doi.org/10.1016/S0142-1123(99)00007-9

[24] el Haddad, M. H., Smith, K. N., & Topper, T. H. (1979). Fatigue Crack Propagation of Short Cracks. *Journal of Engineering Materials and Technology*, *101*(1), 42–46. https://doi.org/10.1115/1.3443647

[25] Dantas, R., Correia, J., Lesiuk, G., Rozumek, D., Zhu, S.-P., de Jesus, A., Susmel, L., & Berto, F. (2021). Evaluation of multiaxial high-cycle fatigue criteria under proportional loading for S355 steel. *Engineering Failure Analysis*, *120*, 105037. https://doi.org/10.1016/j.engfailanal.2020.105037

[26] Mendez-Morales, M., Jesus, J. S., Branco, R., Tankova, T., & Rebelo, C. (2025). Fatigue crack growth of untreated and heat-treated WAAM ER70S-6 carbon steel. *International Journal of Fatigue*, *198*, 109008. https://doi.org/10.1016/j.ijfatigue.2025.109008